A Parametrization of Real Compton Scattering
RPC Technical Note #17

Keith Griffioen
College of William and Mary

July 9, 2001

1 Introduction

In an effort to better simulate real photon experiments with beam energies in the range of 1-50 GeV on nuclear targets, we have set out to model Compton scattering from polarized and unpolarized targets. We break up the discussion into elastic and deep-inelastic scattering from the proton and scattering from atomic electrons.

2 Elastic Compton Scattering from the Proton

Although some earlier data exist[1], we have used only data that is published in tabular form[8, 7, 3, 4, 6, 5]. This data set will be expanded in the future by Jefferson Lab Hall A experiment *Exclusive Compton Scattering on the Proton*, E97-108[9]. Although the data are not necessarily in the perurbative region of QCD, we use dimensional scaling[2] such that the observed cross sections $d\sigma/dt$ go roughly as s^{-6} in which s is the center-of-mass energy squared.

2.1 Kinematics

In the laboratory frame, a real photon with 4-momentum $k^\mu = (k, 0, 0, k)$ strikes a proton at rest with 4-momentum $p^\mu = (M, 0, 0, 0)$. The photon scatters elastically through an angle θ and emerges with 4-momentum $k'^\mu = (k', k' \sin\theta, 0, k' \cos\theta)$. In the center of momentum frame, the incident photon's 4-momentum is $(k^*, 0, 0, k^*)$, the incident proton's 4-momentum is $(\sqrt{M^2 + k^{*2}}, 0, 0, -k^*)$, and the final photon's 4-momomentum is $(k^*, k^* \sin\theta^*, 0, k^* \cos\theta^*)$. The transverse momentum of the photon is the same in both frames and is given by

$$k_\perp = k' \sin\theta = k^* \sin\theta^* \tag{1}$$

The center of mass energy can be evaluated in both frames, and yields

$$s = M^2 + 2Mk = \left(k^* + \sqrt{M^2 + k^{*2}}\right)^2 \tag{2}$$

Therefore,

$$k^* = \frac{s - M^2}{2\sqrt{s}} = \frac{kM}{\sqrt{M^2 + 2kM}} \tag{3}$$

The squared 4-momentum transfer of the photon to the proton can also be evaluated in both reference frames:

$$-t = 4kk' \sin^2 \frac{\theta}{2} = 4k^{*2} \sin^2 \frac{\theta^*}{2} \tag{4}$$

An alternate expression for t arises from the fact that the scattering is elastic, and the square of the final proton 4-momentum $(p^\mu + k^\mu - k'^\mu)$ must be M^2:

$$-t = 2M(k - k') \tag{5}$$

In order to convert between the Lorentz-invariant cross section $d\sigma/dt$ and the experimentally observable lab cross section $d\sigma/d\Omega$, we need to determine the Jacobian for the variable change. Using Eqs. 4 and 5, we can solve for k':

$$k' = \frac{Mk}{M + 2k \sin^2 \frac{\theta}{2}} \tag{6}$$

Plugging this back into Eq. 4 yields

$$-t = \frac{2Mk^2(1 - \cos\theta)}{M + k(1 - \cos\theta)} \tag{7}$$

Differentiating both sides produces

$$\pi dt = k'^2 d\Omega \tag{8}$$

in which $2\pi d\Omega = \sin\theta d\theta$. In the center of momentum frame, the Jacobian is even simpler to work out:

$$-t = \frac{(2 - M^2)^2}{2s}(1 - \cos\theta^*) \tag{9}$$

and

$$\pi dt = \frac{(kM)^2}{2kM + M^2} d\Omega^* \tag{10}$$

in which we have we again have used the fact that $d\sigma/d\Omega$ does not depend on azimuthal angle ϕ, so $\int d\sigma/d\Omega d\phi = 2\pi d\sigma/d\Omega = d\sigma/d(\cos\theta)$, and $d\Omega = 2\pi d(\cos\theta)$. The differential cross sections in Duda, *et al.*, check out as being center-of-mass cross sections, not laboratory cross sections.

2.2 Data

The data in Tables 1–7 are those used in our phenomenological fit. They are specified in terms of the incident photon energy k and the squared 4-momentum transfer t. The last 5 columns are the related kinematic variables of the previous section as calculated from the formulae there.

2.3 The Fit

Although naively one might expect to find scaling in the Lorentz invariants s and $-t$, Fig. 1 shows that this is not the case. As observed in Shupe, the data scale much better with the center-of-mass scattering angle θ^* and s. This is what we used in the following analysis.

The procedure for fitting was as follows. The data (in directory **/afs/slac.stanford.edu/u/ra/griff/comptor** were typed into the files **shupe79**, **deutsch73 anderson70**, **boyarski71**, **breakstone81** and **duda83**. Using the program **kfilter** within the script **cmp_step1.sh** the headers were stripped

Table 1: Real Compton scattering data from Shupe *et al.*[4]. The first four columns are from Shupe, and the rest are calculated from the kinematics.

k GeV	$-t$ GeV^2	$d\sigma/dt$ nb/GeV^2	$\Delta d\sigma/dt$ nb/GeV^2	s GeV^2	k^* GeV	θ^* rad	θ rad	k' GeV
2	1.52	9.5	1.6	4.63344	0.87178	1.5708	0.822116	1.19
2	2.45	4	1.3	4.63344	0.87178	2.22918	1.45257	0.694408
3	0.71	27.5	2.2	6.50999	1.10321	0.783683	0.301598	2.62164
3	1.22	6.9	1.1	6.50999	1.10321	1.04858	0.419064	2.34987
3	2.43	0.97	0.19	6.50999	1.10321	1.56909	0.70367	1.70507
3	3.06	0.55	0.11	6.50999	1.10321	1.83082	0.892383	1.36934
3	3.65	0.51	0.1	6.50999	1.10321	2.0938	1.13366	1.05494
4	0.98	9.4	1	8.38653	1.29598	0.783771	0.266205	3.47776
4	1.68	1.8	0.3	8.38653	1.29598	1.04735	0.369906	3.10474
4	2.49	0.26	0.06	8.38653	1.29598	1.30909	0.487382	2.67309
4	3.36	0.2	0.06	8.38653	1.29598	1.57106	0.626798	2.20947
4	4.23	0.11	0.03	8.38653	1.29598	1.83305	0.799396	1.74586
5	2.45	0.14	0.04	10.2631	1.4644	1.12767	0.366231	3.69441
5	4.29	0.2	0.009	10.2631	1.4644	1.57104	0.569958	2.71388
6	2.45	0.17	0.02	12.1396	1.61576	1.01128	0.296008	4.69441

from these files and the cross sections in **deutsch73, anderson70** and **boyarski71** were multiplied by 1000 so that all cross sections were in nb/GeV^2; the result was written into **cmp_step1.out**. This file served as the input to the program **comkin** called from the script **cmp_step2.sh** which calculated the full kinematics as listed in the tables above. The output of **cmp_step2.sh** was stored in the file **cmp_step2.out**. The perl-script **cmp_step3.pl** read in data from **cmp_step2.out**, scaled the cross sections by s^n for which n was specified on the input line, calculated the logarithm of the cross section and the associated error, and printed out triplets $(\cos\theta^*, \log(d\sigma/td), \{\log(d\sigma/dt+\Delta d\sigma/dt) - \log(d\sigma/dt - \Delta d\sigma/dt))/2\}$. These triplets were fit to a 3rd order polynomial in PAW using the kumac **cmp_step3.kumac**..

This fit was repeated for different values of the exponent n. Although the best fit was for $n < 5$, we chose $n = 6$ to coorespond to the perturbative QCD prediction. With n fixed at this value, we generated 6 coefficients using PAW as shown in Table 9 in which the fit function was of the form $e^{p_1+p_2x} + e^{p_3+p_4x} + e^{p_5+p_6x}$. The χ^2 per degree of freedom was 278 with 198 points.

The PERL script **cmp_step4.pl** creates the plot of $\log(s^n d\sigma/dt)$ versus $\cos\theta^*$ together with the exponents specified in Table 9. Fig. 2 shows all the data used in the fit. Although the cross section probably does not decrease at $\cos\theta^* = -1$, there are few data here to constrain the fit.

The parametrization is coded in the C routine **compton.c**. It accepts incident photon energy k in GeV and 4-momentum tranfer $-t$ in GeV^2, and prints out all kinematic variables, $d\sigma/dt$ and $d\sigma/d\Omega$. This code was modified slightly in **cmp_step6.c** and used in conjuction with the shell script **cmp_step6.sh** to generate the file **cmp_step6.td** and Fig. 3. This figure shows the cross section $d\sigma/d\Omega$ in nb/sr as a function of laboratory scattering angle θ for incident photon energies of $k = 5, 10, 15, 20, 25, 30, 35, 40, 45$ and 50 GeV.

Table 2: Real Compton scattering data from Anderson *et al.*[8]. The first four columns are from Anderson, and the rest are calculated from the kinematics.

k GeV	$-t$ GeV^2	$d\sigma/dt$ nb/GeV^2	$\Delta d\sigma/dt$ nb/GeV^2	s GeV^2	k^* GeV	θ^* rad	θ rad	k' GeV
5.5	0.1	424	44	11.2013	1.5419	0.205451	0.0577846	5.44671
5.5	0.15	355	30	11.2013	1.5419	0.251848	0.0709501	5.42007
5.5	0.2	225	17	11.2013	1.5419	0.291067	0.0821341	5.39342
5.5	0.3	141	15	11.2013	1.5419	0.35712	0.101109	5.34013
5.5	0.4	64.8	5.6	11.2013	1.5419	0.413111	0.117354	5.28684
5.5	0.5	41	3.3	11.2013	1.5419	0.462711	0.131893	5.23355
5.5	0.6	23	4.1	11.2013	1.5419	0.507803	0.145245	5.18026
8.5	0.1	309	39	16.831	1.94399	0.16285	0.0373226	8.44671
8.5	0.2	179	15	16.831	1.94399	0.23056	0.0529525	8.39342
8.5	0.3	114	11	16.831	1.94399	0.282693	0.0650641	8.34013
8.5	0.4	53.8	4.6	16.831	1.94399	0.326792	0.0753753	8.28684
8.5	0.5	34.3	2.7	16.831	1.94399	0.365776	0.0845495	8.23355
8.5	0.6	19.1	1.8	16.831	1.94399	0.401142	0.0929263	8.18026
8.5	0.7	10.5	1.1	16.831	1.94399	0.433777	0.100707	8.12697
8.5	0.8	8.53	1.5	16.831	1.94399	0.464258	0.108022	8.07368
11.5	0.06	441	63	22.4606	2.27675	0.107639	0.02133	11.468
11.5	0.1	334	28	22.4606	2.27675	0.139006	0.0275629	11.4467
11.5	0.2	171	11	22.4606	2.27675	0.196743	0.0390721	11.3934
11.5	0.3	95.2	9	22.4606	2.27675	0.241156	0.0479672	11.3401
11.5	0.4	49.9	4.1	22.4606	2.27675	0.278689	0.0555201	11.2868
11.5	0.5	31.2	2.6	22.4606	2.27675	0.311839	0.0622225	11.2336
11.5	0.6	16.5	1.5	22.4606	2.27675	0.341883	0.0683259	11.1803
11.5	0.7	9	0.98	22.4606	2.27675	0.369579	0.0739794	11.127
11.5	0.8	5.5	0.7	22.4606	2.27675	0.395423	0.07928	11.0737
17	0.1	302	23	32.7816	2.78588	0.113572	0.0186311	16.9467
17	0.2	143	8.8	32.7816	2.78588	0.160701	0.0263903	16.8934
17	0.3	85	7	32.7816	2.78588	0.196925	0.032373	16.8401
17	0.4	48	4.6	32.7816	2.78588	0.227512	0.0374409	16.7868
17	0.5	26.6	2.4	32.7816	2.78588	0.254504	0.0419274	16.7336
17	0.6	15.3	1.3	32.7816	2.78588	0.278947	0.0460032	16.6803
17	0.7	7.6	1.6	32.7816	2.78588	0.301462	0.0497694	16.627
17	0.8	5.7	0.63	32.7816	2.78588	0.322452	0.053292	16.5737
17	0.9	3.26	0.37	32.7816	2.78588	0.3422	0.0566167	16.5204
17	1.1	1.38	0.22	32.7816	2.78588	0.378732	0.0627969	16.4138

Table 3: Real Compton scattering data from Boyarski *et al.*[7]. The first four columns are from Boyarski, and the rest are calculated from the kinematics.

k GeV	$-t$ GeV^2	$d\sigma/dt$ nb/GeV^2	$\Delta d\sigma/dt$ nb/GeV^2	s GeV^2	k^* GeV	θ^* rad	θ rad	k' GeV
8	0.014	660	50	15.8927	1.88287	0.0628515	0.0147972	7.99254
8	0.025	710	40	15.8927	1.88287	0.0839997	0.019781	7.98668
8	0.047	590	30	15.8927	1.88287	0.115204	0.0271427	7.97495
8	0.078	430	30	15.8927	1.88287	0.148466	0.0350034	7.95843
8	0.119	315	20	15.8927	1.88287	0.183469	0.0432958	7.93659
8	0.169	223	15	15.8927	1.88287	0.218771	0.0516845	7.90994
16	0.025	590	40	30.9051	2.70044	0.0585596	0.00988627	15.9867
16	0.047	489	21	30.9051	2.70044	0.080303	0.0135604	15.975
16	0.078	348	15	30.9051	2.70044	0.103468	0.0174782	15.9584
16	0.119	271	13	30.9051	2.70044	0.127831	0.0216035	15.9366
16	0.169	185	11	30.9051	2.70044	0.152381	0.0257668	15.9099

Table 4: Real Compton scattering data from Breakstone *et al.*[6]. The first four columns are from Breakstone, and the rest are calculated from the kinematics. Breakstone quotes ranges for k and $-t$. We have taken the middle of the k-range and calculated the $-t$ assuming a distribution of the form e^{-7t} as suggested by the paper.

k GeV	$-t$ GeV^2	$d\sigma/dt$ nb/GeV^2	$\Delta d\sigma/dt$ nb/GeV^2	s GeV^2	k^* GeV	θ^* rad	θ rad	k' GeV
62	0.084	328	64	117.226	5.37289	0.0539491	0.00467633	61.9552
62	0.124	214	36	117.226	5.37289	0.0655511	0.00568266	61.9339
62	0.19	146	21	117.226	5.37289	0.0811498	0.00703624	61.8988
62	0.305	63.5	9.7	117.226	5.37289	0.102833	0.00891928	61.8375
62	0.501	15.2	3.6	117.226	5.37289	0.131833	0.0114411	61.733
62	0.827	0.62	0.5	117.226	5.37289	0.169459	0.0147202	61.5593
85	0.084	284	72	160.387	6.29743	0.0460272	0.00341064	84.9552
85	0.124	213	44	160.387	6.29743	0.0559247	0.00414439	84.9339
85	0.19	150	26	160.387	6.29743	0.0692309	0.00513118	84.8988
85	0.305	57.6	11	160.387	6.29743	0.0877254	0.0065035	84.8375
85	0.501	24.5	5.9	160.387	6.29743	0.112456	0.00834035	84.733
85	0.827	1.61	1.3	160.387	6.29743	0.144533	0.0107267	84.5593
112	0.124	234	46	211.053	7.23354	0.0486859	0.003145	111.934
112	0.19	145	24	211.053	7.23354	0.0602687	0.00389364	111.899
112	0.305	54.2	11	211.053	7.23354	0.0763668	0.00493455	111.837
112	0.501	15.3	3.7	211.053	7.23354	0.0978907	0.00632732	111.733
112	0.827	2.77	1.8	211.053	7.23354	0.125802	0.00813565	111.559

Table 5: Real Compton scattering data from Duda *et al.*[5]. The first four columns are from Duda, and the rest are calculated from the kinematics.

k GeV	$-t$ GeV^2	$d\sigma/dt$ nb/GeV^2	$\Delta d\sigma/dt$ nb/GeV^2	s GeV^2	k^* GeV	θ^* rad	θ rad	k' GeV
1.243	0.171	512	48	3.2129	0.650656	0.646759	0.347332	1.15188
1.236	0.219	554	44	3.19976	0.648318	0.738496	0.400541	1.1193
1.233	0.268	307	35	3.19413	0.647314	0.822757	0.45031	1.09018
1.226	0.327	241	44	3.181	0.644967	0.918573	0.509065	1.05174
1.211	0.446	303	33	3.15285	0.639914	1.09795	0.625264	0.973329
1.219	0.581	84	24	3.16786	0.642613	1.26974	0.740777	0.909388
1.225	0.718	87	40	3.17912	0.644631	1.43429	0.86044	0.842382
1.321	0.18	561	48	3.35927	0.676253	0.638148	0.335071	1.22508
1.314	0.231	462	35	3.34613	0.673989	0.729151	0.386615	1.1909
1.315	0.285	355	31	3.34801	0.674312	0.813988	0.435088	1.16313
1.311	0.349	224	30	3.3405	0.673016	0.908729	0.491371	1.12502
1.304	0.473	188	25	3.32737	0.670743	1.0766	0.595996	1.05194
1.308	0.625	66	14	3.33487	0.672043	1.25762	0.715226	0.974941
1.311	0.774	40	23	3.3405	0.673016	1.42467	0.834602	0.89854
1.406	0.187	628	40	3.51878	0.703264	0.625021	0.320449	1.30635
1.405	0.242	582	35	3.5169	0.702951	0.714943	0.369497	1.27604
1.405	0.298	335	29	3.5169	0.702951	0.797544	0.415533	1.2462
1.404	0.367	218	26	3.51502	0.702638	0.891408	0.46939	1.20843
1.399	0.499	121	12	3.50564	0.701072	1.05598	0.568693	1.13309
1.401	0.662	58	11	3.50939	0.701699	1.23687	0.684699	1.04822
1.404	0.826	30	14	3.51502	0.702638	1.4066	0.802653	0.963829
1.488	0.193	643	48	3.67265	0.728521	0.612559	0.307212	1.38515
1.494	0.25	505	29	3.68391	0.730339	0.698741	0.352494	1.36078
1.498	0.311	299	24	3.69142	0.73155	0.782099	0.397365	1.33227
1.495	0.384	165	21	3.68579	0.730642	0.875855	0.449943	1.29037
1.49	0.53	104	14	3.6764	0.729127	1.04543	0.549629	1.20757
1.498	0.698	42	8	3.69142	0.73155	1.2155	0.654914	1.12604
1.5	0.873	30	11	3.69517	0.732155	1.384	0.768748	1.03478
1.56	0.2	556	38	3.80776	0.750099	0.60541	0.298103	1.45342
1.574	0.26	443	28	3.83403	0.754233	0.689639	0.340875	1.43545
1.585	0.324	298	24	3.85468	0.757468	0.770374	0.382774	1.41234
1.581	0.402	152	18	3.84717	0.756293	0.865068	0.434734	1.36678
1.576	0.563	67	13	3.83779	0.754822	1.04034	0.535495	1.27598
1.59	0.736	32	6	3.86406	0.758934	1.20136	0.632128	1.19779
1.594	0.925	20	10	3.87157	0.760105	1.36995	0.742939	1.10107
1.622	0.206	513	56	3.92411	0.768262	0.599726	0.290825	1.51222
1.641	0.269	406	24	3.95976	0.773754	0.683536	0.332367	1.49765
1.663	0.337	306	24	4.00105	0.780071	0.762524	0.371742	1.48341
1.658	0.423	132	20	3.99166	0.778639	0.861697	0.425201	1.43259
1.652	0.594	68	22	3.98041	0.776918	1.03799	0.524892	1.33546
1.676	0.779	13	3	4.02544	0.783783	1.19613	0.616885	1.26088

Table 6: Real Compton scattering data from Deutsch *et al.*[3]. The first four columns are from Deutsch, and the rest are calculated from the kinematics.

k GeV	$-t$ GeV^2	$d\sigma/dt$ nb/GeV^2	$\Delta d\sigma/dt$ nb/GeV^2	s GeV^2	k^* GeV	θ^* rad	θ rad	k' GeV
0.57	0.147	1100	106	1.94998	0.382991	1.04845	0.74109	0.491665
0.6	0.158	895	85	2.00628	0.397452	1.04732	0.73066	0.515803
0.63	0.169	1425	102	2.06258	0.411589	1.04581	0.720328	0.539941
0.66	0.181	1682	107	2.11887	0.425422	1.04725	0.712574	0.563546
0.69	0.193	1568	101	2.17517	0.438966	1.04812	0.704698	0.587151
0.72	0.205	1492	98	2.23147	0.452237	1.04856	0.696784	0.610757
0.75	0.216	2101	101	2.28776	0.465248	1.04598	0.686939	0.634895
0.78	0.229	1810	115	2.34406	0.478012	1.04847	0.681075	0.657967
0.81	0.241	1516	111	2.40035	0.490542	1.04808	0.673358	0.681572
0.84	0.253	1410	116	2.45665	0.502847	1.04753	0.665767	0.705178
0.565	0.412	1744	190	1.9406	0.380548	2.00699	1.62627	0.345447
0.595	0.444	1560	166	1.9969	0.395064	2.00687	1.61186	0.358395
0.625	0.476	1683	167	2.05319	0.409255	2.00533	1.59627	0.371342
0.655	0.509	1469	153	2.10949	0.423137	2.00582	1.58329	0.383757
0.685	0.542	1339	147	2.16579	0.436728	2.00517	1.56941	0.396171
0.715	0.576	1472	160	2.22208	0.450044	2.00639	1.55792	0.408053
0.745	0.61	1075	146	2.27838	0.463097	2.00665	1.5457	0.419934
0.775	0.644	982	153	2.33468	0.475902	2.00616	1.53297	0.431816
0.805	0.679	804	154	2.39097	0.488469	2.00741	1.52243	0.443165
0.85	0.26	1257	135	2.47542	0.506901	1.05404	0.668055	0.711447
0.9	0.28	908	100	2.56924	0.526828	1.05229	0.655389	0.75079
0.95	0.3	796	89	2.66307	0.546212	1.05039	0.643223	0.790132
1	0.32	798	87	2.7569	0.565091	1.04841	0.631561	0.829474
1.05	0.34	542	70	2.85073	0.583499	1.0464	0.620395	0.868816
1.1	0.36	387	60	2.94455	0.601467	1.04438	0.609708	0.908158
1.15	0.38	355	60	3.03838	0.619021	1.04239	0.599482	0.9475
1.2	0.4	280	58	3.13221	0.636187	1.04043	0.589694	0.986842
1.25	0.43	239	60	3.22603	0.652987	1.05208	0.588969	1.02086
0.7	0.242	1300	127	2.19394	0.44342	1.17602	0.799181	0.57104
0.75	0.263	1363	121	2.28776	0.465248	1.16746	0.777746	0.609849
0.8	0.283	1114	106	2.38159	0.486391	1.15722	0.756059	0.649191
0.85	0.304	1058	103	2.47542	0.506901	1.15005	0.737604	0.688
0.9	0.325	910	95	2.56924	0.526828	1.14339	0.720346	0.726809
0.95	0.344	782	87	2.66307	0.546212	1.1335	0.701539	0.766684
1	0.364	640	80	2.7569	0.565091	1.12625	0.685345	0.806026
1.05	0.384	428	65	2.85073	0.583499	1.11956	0.670203	0.845369
1.1	0.402	449	67	2.94455	0.601467	1.11031	0.653913	0.885776
1.15	0.421	315	58	3.03838	0.619021	1.10329	0.639734	0.925651
1.2	0.439	294	59	3.13221	0.636187	1.09543	0.625523	0.966059

Table 7: Same as Table 6

k GeV	$-t$ GeV^2	$d\sigma/dt$ nb/GeV^2	$\Delta d\sigma/dt$ nb/GeV^2	s GeV^2	k^* GeV	θ^* rad	θ rad	k' GeV
1.25	0.457	187	53	3.22603	0.652987	1.08817	0.612219	1.00647
1.138	0.463	300	26	3.01586	0.614845	1.17275	0.689199	0.89127
1.213	0.494	249	23	3.1566	0.640589	1.16137	0.667133	0.94975
1.288	0.524	144	18	3.29734	0.665522	1.15002	0.646244	1.00876
1.363	0.553	118	16	3.43808	0.68971	1.13873	0.626457	1.06831
1.438	0.582	125	16	3.57882	0.71321	1.12861	0.608378	1.12786
1.513	0.61	86.7	14	3.71957	0.736074	1.11846	0.591141	1.18793
1.588	0.636	66.1	12	3.86031	0.758348	1.10734	0.574102	1.24908
1.663	0.663	61.4	12	4.00105	0.780071	1.09817	0.558979	1.30969
1.738	0.687	51.8	12	4.14179	0.801281	1.08717	0.543437	1.3719
1.813	0.713	45.8	12	4.28253	0.822009	1.07879	0.530044	1.43305
1.888	0.736	72.9	17	4.42327	0.842285	1.06868	0.516221	1.49579
1.5	0.692	85.6	12	3.69517	0.732155	1.20838	0.649984	1.13124
1.7	0.773	45.9	6.7	4.07048	0.790597	1.17922	0.603254	1.28807
1.9	0.85	39.1	6.2	4.44579	0.845489	1.1533	0.563446	1.44704
2.1	0.92	20.7	4.5	4.8211	0.897377	1.12766	0.527788	1.60974
2.3	0.986	18.5	4.3	5.19641	0.946684	1.10414	0.496592	1.77457
2.5	1.048	7.5	2.8	5.57171	0.993744	1.08221	0.468949	1.94153
1.45	0.14	500	50	3.60134	0.71691	0.528028	0.265733	1.37539
1.6	0.178	530	50	3.88282	0.761859	0.561109	0.272714	1.50514
1.8	0.213	350	40	4.25813	0.818449	0.571647	0.265668	1.68649
1.98	0.248	330	40	4.59591	0.866579	0.582886	0.261093	1.84784
2.1	0.29	280	50	4.8211	0.897377	0.60949	0.267221	1.94546
2.4	0.162	400	30	5.38406	0.970477	0.417768	0.171014	2.31367
2.7	0.201	280	30	5.94702	1.03883	0.434996	0.169647	2.59289
3	0.238	280	30	6.50999	1.10321	0.445895	0.16636	2.87317
3.1	0.275	190	30	6.69764	1.1239	0.470931	0.173526	2.95345
2.4	0.162	350	60	5.38406	0.970477	0.417768	0.171014	2.31367
2.7	0.201	300	30	5.94702	1.03883	0.434996	0.169647	2.59289
3	0.243	220	30	6.50999	1.10321	0.450634	0.16818	2.87051
3.4	0.29	200	30	7.2606	1.18392	0.458875	0.162292	3.24546
3.75	0.34	210	40	7.91739	1.25046	0.470637	0.159559	3.56882
2	0.162	480	50	4.63344	0.87178	0.465892	0.2061	1.91367
2.2	0.201	420	40	5.00875	0.922331	0.491001	0.209318	2.09289
2.45	0.243	370	50	5.47789	0.982174	0.50732	0.207112	2.32051
2.65	0.29	180	30	5.8532	1.02773	0.530175	0.209796	2.49546
2.85	0.34	160	30	6.2285	1.07147	0.551148	0.211821	2.66882
3.4	0.162	360	30	7.2606	1.18392	0.341625	0.119984	3.31367
3.75	0.201	260	30	7.91739	1.25046	0.360482	0.121374	3.64289

Table 8: Same as Table 6

k	$-t$	$d\sigma/dt$	$\Delta d\sigma/dt$	s	k^*	θ^*	θ	k'
GeV	GeV^2	nb/GeV^2	nb/GeV^2	GeV^2	GeV	rad	rad	GeV
4.15	0.243	190	30	8.66801	1.32257	0.374915	0.120754	4.02051
4.6	0.29	180	40	9.51246	1.39939	0.387236	0.119157	4.44546
2.7	0.162	350	30	5.94702	1.03883	0.389915	0.151658	2.61367
3.1	0.201	320	30	6.69764	1.1239	0.401597	0.147321	2.99289
3.4	0.243	240	30	7.2606	1.18392	0.41944	0.147963	3.27051
3.7	0.29	200	40	7.82357	1.24116	0.437359	0.14882	3.54546
3.1	0.28	200	20	6.69764	1.1239	0.475275	0.17518	2.95079
3.25	0.3	180	20	6.97912	1.15428	0.479082	0.17305	3.09013
3.43	0.34	140	20	7.3169	1.18976	0.495137	0.174897	3.24882
3.62	0.37	140	10	7.67344	1.22615	0.501321	0.17302	3.42283
3.82	0.41	110	15	8.04875	1.26336	0.51242	0.172846	3.60151

Table 9: Polynomial fit parameters as generated by PAW.

NO.	NAME	VALUE	ERROR	STEP	DERIVATIVE
1	P1	2.4699	0.28582E-06	0.62484E-03	-55.666
2	P2	0.10181	0.35771E-06	0.22563E-03	-807.59
3	P3	-9.0315	0.50572E-06	0.22848E-02	-2991.2
4	P4	11.659	0.51502E-06	0.29496E-02	-3515.0
5	P5	-5.8482	0.57629E-06	14.795	0.35308
6	P6	-3.7345	0.19953E-01	4.7742	-0.47079

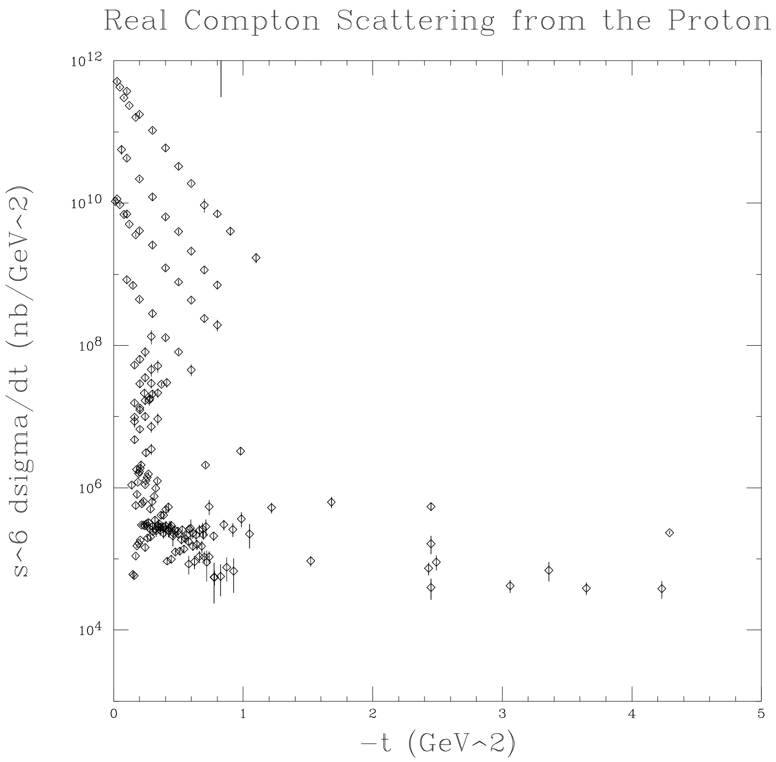

Figure 1: Compton scattering data scaled with s^6 plotted versus $-t$.

2.4 Predictions for Photon Experiments

Fig. 4 shows calculations of the expected cross sections as a function of the scattered photon energy k' for various small angles less than 10 degrees. Incident photons ranged from $k = 10$ to 50 GeV, weighted by $1/k$ for a bremsstrahlung-like spectrum of initial photons. These were generated with the program **cmpt.c** and plotted with the script **cmpt.pl**.

For the sake of the calculation, we assume 10^5 incident photons per second with a $1/k$ distribution extending from 10 to 50 GeV. In order to calculate the probability of a given photon energy, we assume the probability distribution $1/k \log(k_{max}/k_{min})$. With $\delta k = (50-10)/100 = 0.4$ GeV, we obtain $2.49 \times 10^4/k$ incident photons of energy k per second. The scattering cross section $d\sigma/d\theta = MN_s/\rho N_A N_i \Delta\theta$ in which M is the molar mass of the target, N_s is the number of scattered particles, ρ is the areal density of the target, N_A is Avogadro's number, N_i is the number of incident particles and $\Delta\theta$ is the angular acceptance of the detector in degrees (assuming it covers a whole annulus around the beam direction). For a LiD target we can estimate $M/\rho/N_A \approx 1.7 \times 10^{-24}$ cm^2 which is $1.7 \times 10^9 nb$. We take $\Delta\theta = 1°$, so $N_s = d\sigma/d\theta/k$ (nb/deg/GeV) 2.49×10^4 GeV $1°/1.7 \times 10^9$ nb $= 1.46 \times 10^{-5} d\sigma/d\theta/k$.

Fig. 5 shows the expected counting rates for a full annulus at increments of 1 degree for the estimated target and beam parameters listed above. If we sum the number of photons per second at any energy and fixed angle we obtain 9.2 3.2 0.47 0.055 0.0075 0.0015 0.0005 0.0002 0.0001 for the angles 1 2 3 4 5 6 7 8 9 degrees. The integrated energy per second is correspondingly 115 37 5.2 0.59 0.080 0.016 0.005 0.002 0.001 GeV.

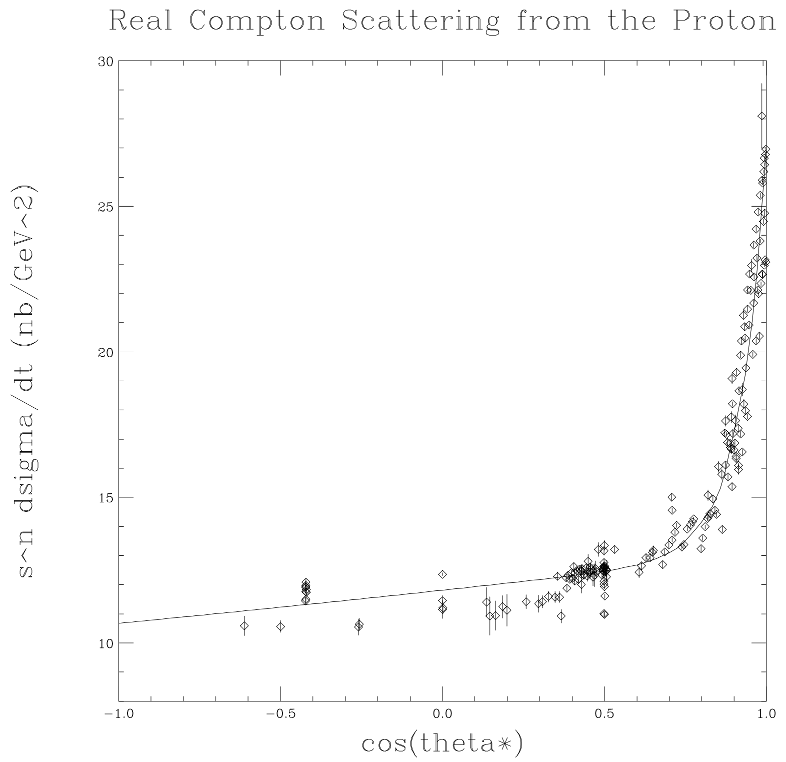

Figure 2: Logarithm of the Compton scattering data scaled by $s^{5.25}$ versus $\cos\theta^*$ together with the polynomial fit.

3 Compton Scattering from an Electron

The kinematics of the previous section applies equally well to electron targets if the nucleon mass M is replaced by the electron mass m. Tolhoek[10] has worked out the Compton scattering cross sections for the electron. In particular, for circularly polarized electrons and longitudinally polarized electrons, the Compton scattering cross section for a photon hitting an electron at rest is

$$\frac{d\sigma}{d\Omega} = \frac{d\sigma_u}{d\Omega} + P_b P_t \frac{d\sigma_p}{d\Omega} \tag{11}$$

in which P_b is the photon beam polarization, P_t is the electron target polarization, and $\sigma_{u,p}$ is the unpolarized and polarized cross sections.

$$\frac{d\sigma_u}{d\Omega} = \frac{1}{2}\frac{\alpha^2}{m^2}\left(\frac{k'}{k}\right)^2 \left[1 + \cos^2\theta + \frac{(k-k')}{m}(1-\cos\theta)\right] \tag{12}$$

which, with the kinematic constraint that $2m(k-k') = 2kk'(1-\cos\theta)$, is equivalent to the more standard Klein-Nishina form

$$\frac{d\sigma_u}{d\Omega} = \frac{1}{2}\frac{\alpha^2}{m^2}\left(\frac{k'}{k}\right)^2 \left[\frac{k'}{k} + \frac{k}{k'} - \sin^2\theta\right] \tag{13}$$

The polarized cross section is

$$\frac{d\sigma_p}{d\Omega} = \frac{1}{2}\frac{\alpha^2}{m^2}\left(\frac{k'}{k}\right)^2 \left[(1-\cos^2\theta)\cos\theta\frac{(k+k')}{m}\right] \tag{14}$$

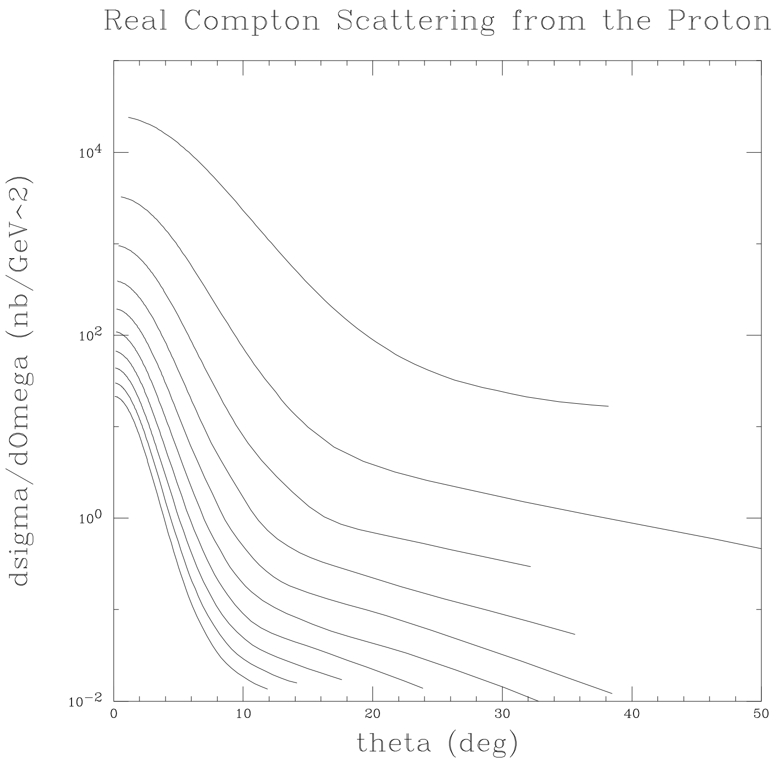

Figure 3: Cross sections for Compton scattering at incident energies 5, 10, 15, 20, 25, 30, 35, 40, 45, and 50 GeV as a function of laboratory scattering angle θ. The upper curve is $k = 5$ GeV and the lower curve is $k = 50$ GeV.

in which right circularly polarized photons and electrons spins parallel to $\mathbf{k}$ correspond to the positive polarizations.

If we wish to calculate for $\theta^* = 90^\circ$, we find that $\sin\theta^* = 1$ and $\sin\theta = k^*/k'$. We take the limit in which $k \gg m$, such that $k^* = km/\sqrt{m^2+2mk} \approx \sqrt{km/2}$, $\sin\theta \approx \theta$, $\cos\theta \approx 1-\theta^2/2$, $k' = mk\sin\theta/(m+k(1-\cos\theta)) \approx mk\theta/(m+k\theta^2/2)$. This gives the quadratic equation $k\theta^2/2 - \sqrt{2mk}\theta + m = 0$ for which $\theta = \sqrt{2m/k}$. For the photon energies $k = 10, 20, 30, 40$, and 50 GeV, this corresponds to 10.1(0.579), 7.1(0.409), 5.8(0.334), 5.1(0.289), and 4.5(0.259) milliradians (degrees), respectively. The unpolarized cross sections are 24.8 mb/sr and the asymmetries are 0.6 for all energies.

By contrast, the Moller scattering cross section in the lab frame (i.e. the target electron is at rest) is

$$\frac{d\sigma_M}{d\Omega} = \frac{1}{4}\frac{\alpha^2}{m^2}\left[\frac{(1+\cos\theta^*)(3+\cos^2\theta^*)}{\sin^2\theta}\right] \tag{15}$$

and the asymmetry for polarizations of both electrons along the beam axis is

$$A_{zz} = -\frac{(7+\cos^2\theta^*)\sin^2\theta^*}{(3+\cos^2\theta^*)} \tag{16}$$

such that at $\theta^* = 90^\circ$ the unpolarized cross section is 179 mb/sr and $A_{zz} = -7/9$. The E155 Moller detector had masks with an acceptance of 0.20–0.22 mrad in ϕ and $3.59 < \theta < 8.96$ mrad. This corresponds to a solid angle of $\Delta\Omega = 6.7 \times 10^{-5}$ sr.

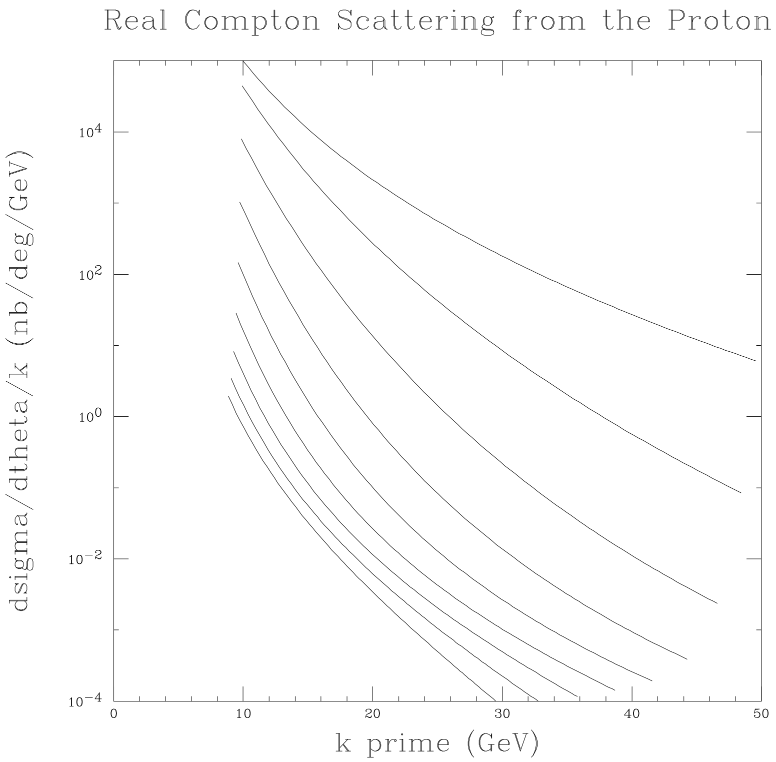

Figure 4: Cross sections (in nb) per opening angle $d\theta$ in degrees divided by a $1/k$ bremsstrahlung-like spectrum (GeV), as a function of k' for scattering angles of 1, 2, 3, 4, 5, 6, 7, 8, 9 degrees. The smallest angles have the largest cross sections.

If we were to build a Compton polarimeter similar to the E155 Moller polarimeter, we can expect the following event rates. For a 100 μm Fe foil, the luminosity L is given by $\rho N_A N_i \epsilon / M$ in which ρ is the areal density of iron (7.87 g/cm^2 $\times$ 0.01 cm), $N_A = 6.02 \times 10^{23}$/mole, N_i is the incident particle rate (10^5/s), ϵ is the number of electrons per atom (26), and M is the molar mass of Fe (56). We find that $L = 2$/mb/s. The Compton counting rate would then be 2/mb/s $\times$ 24.8 mb/sr $\times 6.7 \times 10^{-5}$ sr $= 0.003$/s. The raw asymmetry will be roughly $0.6 \times 0.08 \times 0.5 = 0.024$ in which the terms are respectively the actual asymmetry, the target polarization, and a rough beam polarization. For 250,000 events, we get a statistical error of 8%. A foil of 1cm thickness buys a factor of 100, and the rate becomes 0.3/s. Covering a wider range in ϕ would also help these rates. For a rate of 1/s a 250,000 second Compton run would take 69 hours.

4 Deep-Inelastic Compton Scattering

In this case, the incident 4-momenta are identical to the elastic photon-proton scattering case in the lab frame. However, now the scattered photon energy in the center of momentum frame $k^{*\prime} \neq k^*$ as in the elastic case. Now we find that

$$-t = 4kk' \sin^2 \frac{\theta}{2} = 4k^* k^{*\prime} \sin^2 \frac{\theta^*}{2} \tag{17}$$

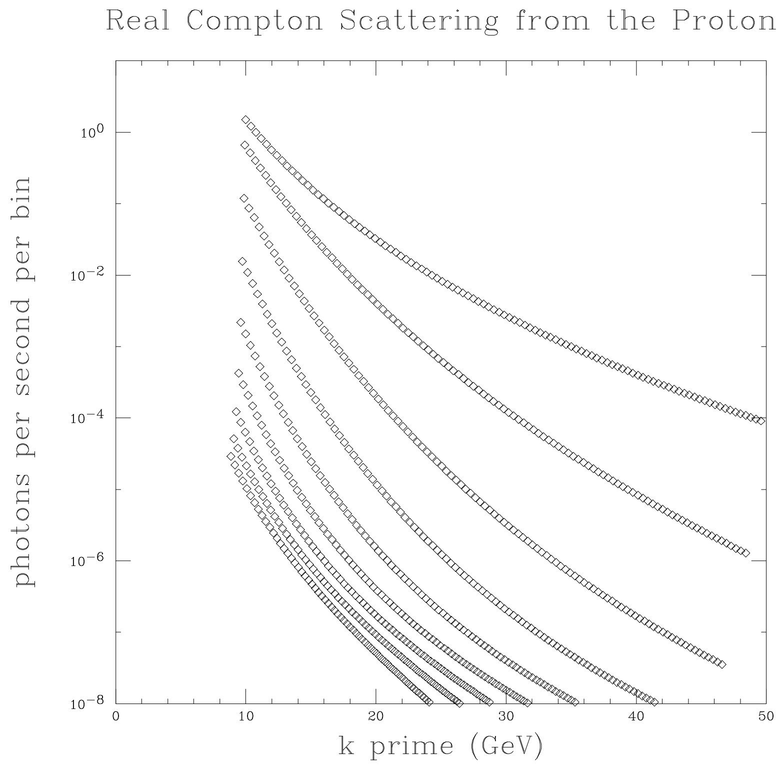

Figure 5: Photons per second per bin (each point), as a function of k' for scattering angles of 1, 2, 3, 4, 5, 6, 7, 8, 9 degrees. The smallest angles have the largest counting rates.

and the transverse momentum

$$k_T = k' \sin\theta = k^{*\prime} \sin\theta^* \tag{18}$$

This leads to the equation

$$k \tan\frac{\theta}{2} = k^* \tan\frac{\theta}{2} \tag{19}$$

Maël[11] has calculated cross sections using very old polarized quark distribution functions and found that deep-inelastic Compton scattering is quite sensitive to the polarized up-quark distribution Δu. The Compton scattering process is given by

$$E' \frac{d^3\Delta\sigma}{dk'^3} = \sum_q \Delta G_{q/p}(x, Q^2) \frac{xs}{(s+u)\pi} \frac{d\Delta\sigma}{d\hat{t}}(\gamma\mathrm{q} \to \gamma q) \tag{20}$$

in which $G_{q/p}$ are the polarized quark distribution functions, and the fundamental quark-photon cross sections are

$$\frac{d\Delta\sigma}{d\hat{t}} = \frac{4\pi\alpha^2 e_q^4}{\hat{s}^2}\left(\frac{\hat{u}}{\hat{s}} - \frac{\hat{s}}{\hat{u}}\right) \tag{21}$$

and

$$\frac{d\sigma}{d\hat{t}} = -\frac{2\pi\alpha^2 e_q^4}{\hat{s}^2}\left(\frac{\hat{u}}{\hat{s}} + \frac{\hat{s}}{\hat{u}}\right) \tag{22}$$

The Mandelstam variables for a reaction $AB \to CD$ are $s = (A+B)^2$, $t = (A-C)^2$, and $u = (A-D)^2$ with $s+t+u = M_A^2 + M_B^2 + M_C^2 + M_D^2$. For Compton scattering the corresponding quark variables are $\hat{s} = xs$, $\hat{t} = t$ and $\hat{u} = xu$. Maël calculates these quantities using the approximation that $k \ll M$ as follows:

$$\hat{s} = xs \qquad \hat{t} = -s\frac{X_T'}{2}e^{-\eta} \qquad \hat{u} = -xs\frac{X_T'}{2}e^{\eta} \tag{23}$$

The momentum fraction x, pseudorapidity η and normalized transverse momentum X_T' are given by

$$x = \frac{X_T'e^{-\eta}}{2 - X_T'e^{\eta}} \qquad \eta = -\ln\tan\frac{\theta^*}{2} \qquad X_T' = \frac{2k_T}{\sqrt{s}} \tag{24}$$

The correct equation for u is

$$u = M^2 - 2Mk \tag{25}$$

If we assume from above that $u = -sX_T'e^{\eta}/2$, we find that $u = -\sqrt{s}k'\sin\theta k^*/(k\tan\frac{\theta}{2}) = -2Mk'\cos^2\frac{\theta}{2}$ which equals $M^2 - 2k'M$ in the limit that M^2 can be neglected at $\theta \approx 0$. The expression $\hat{t} = -sX_T'e^{-\eta}/2 = ts/(s - M^2)$ which reduces to t for $s \gg M^2$. Likewise, $x = X_T'e^{-\eta}/(2 - X_T'e^{\eta} = -tk/[(s - M^2)(k - (s - M^2)k'\cos^2\frac{\theta}{2})] = -t/2M(k - k')$ in the limit of $M^2 \ll k$ and $\theta \approx 0$. The final expression is what we expect from deep-inelastic kinematics.

Corrections to this from photon structure or fragmentation contribute with different signs in the forward region and nearly cancel near $\eta = -\ln X_T'$. In this limit $-t = sX_T'^2/2$ and $x = X_T'^2$. The scale $Q^2 = k_T^2$ is the usual choice for photon photoproduction. In that case $Q^2 = sX_T'/4$.

We can estimate the cross sections using the program `dcompton.c`. For $k' \approx k/2$, $\eta = -\ln X_T'$. The cross sections are on the order of 0.1 nb/GeV^2 for angles around 5 degrees, such that $X_T' > 0.3$ The luminosity L using a LiD target is on the order of 10^{-4} /nb/s. The solid angle of 1° opening at 5 degrees is about 0.1 integrated over ϕ. Therefore, the counting rates are 0.1 nb/GeV$^2\times$ 0.1 GeV^2 $\times\, 10^{-4}$ /nb/s $= 10^{-6}$/s. If this is correct, the rates are too low to contribute significantly.

5 Comparative Cross Sections

Fig. 6 shows the comparative cross sections in nb/sr for the three processes elastic Compton scattering from the proton (solid), Compton scattering from the atomic electrons (dashed), and deep-inelastic Compton scattering from the proton for $k' = 20$ GeV (dotted) and 10 GeV (dot-dashed). The photon beam energy is 30 GeV for all cases.

Fig. 7 is the same as Fig. 6 except for a beam energy of 3 GeV. The nuclear scattering is now comparatively larger because of the corresponding form factors.

Fig. 8 shows the Compton cross sections for $\theta_{lab} = 1°$. The X corresponds to scattering from the atomic electrons, the diamond to elastic proton scattering and the squares to deep-inelastic scattering. Although the deep-inelastic rate is many orders of magnitude smaller than the elastic proton or electron scattering, it can still be separated by looking at the photon energy.

Fig. 9 shows the Compton cross sections for $\theta_{lab} = 3°$. The X corresponds to scattering from the atomic electrons, the diamond to elastic proton scattering and the squares to deep-inelastic scattering. Now the deep-inelastic cross section dominates. In fact, if we demand that $X_T' > 0.2$ then we must look at angles greater than 3°. With the additional constraint that $\eta = -\ln X_T'$, which minimizes the contributions from fragmentation and photon structure, we can make a measure of $\Delta u/u$. In a very conservative estimate, a measurement on a 1 b^{-1} target would require 1 month of continuous running at 10^7 photons per second to obtain errors of less than 10% on the asymmetries over the range of $x from 0.04 to 0.7$. Table 10 lists these estimates. With a

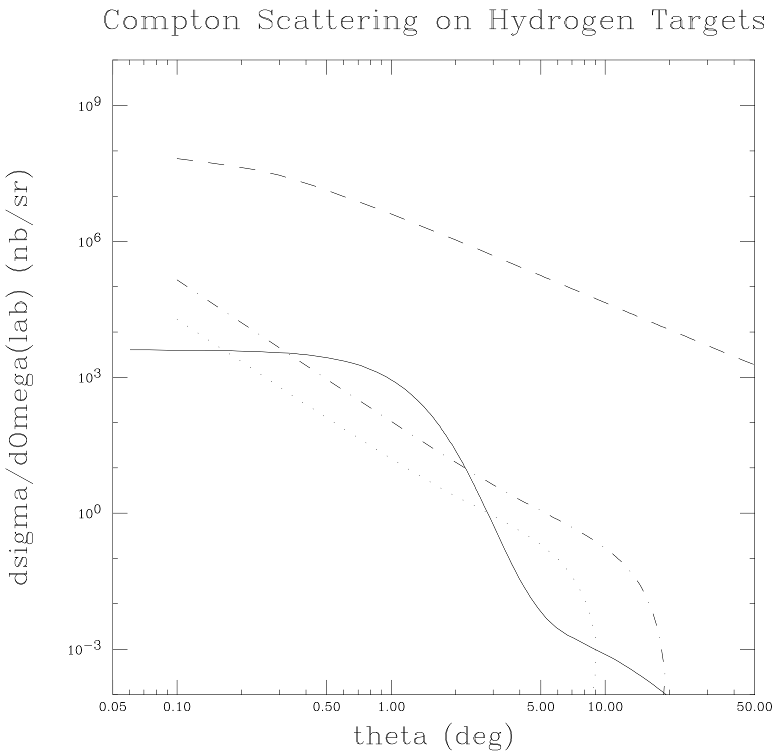

Figure 6: Compton scattering from hydrogen targets with a $k = 30$ GeV beam. See text for explanation of the curves.

proper study over all kinematics (namely, relaxing the constraint that $\eta = -\ln X'_T$), one can use all k' values for a given beam energy, not just a single one. This improves the statistics for one, but allows a sensitivity to the photon structure functions and fragmentation functions as well.

6 Photon Polarization

A diamond crystal radiator is able to produce circularly polarized light from longitudinally polarized electrons. However, there is a component of linearly polarized light that survives. We need to understand the interplay between circular and linear polarization in the beam and what possible uses the linear polarization may have.

Suppose we write the electric field vector of a real photon as $\mathrm{E} = E_0 \epsilon \exp i(kz - \omega t)$ in which the polarization vector ϵ can take a variety of forms. For linear polarization along the x and y axes, $\epsilon_{\mathbf{x}} = (1, 0)$ and $\epsilon_{\mathbf{y}} = (0, 1)$, respectively. For right-handed and left-handed circular polarization $\epsilon_+ = (1, i)/\sqrt{2}$ and $\epsilon_- = (1, -i)/\sqrt{2}$. In this case, the imaginary y-component adds a phase of $\pm\pi/2$ to the complex exponential, converting a cosine to a sine and vice versa. Suppose we take the most general vector $\epsilon = a\epsilon_+ + b\epsilon_-$ with the normalization condition that $\epsilon^* \cdot \epsilon = 1$. This implies that $a^*a + b^*b = 1$. For such a field, we can determine the probability of a photon having linear polarizations along the x or y directions or positive and negative circular polarization. $P_x = (a+b)^*(a+b)/2 = 1 + (a^*b + b^*a)/2$, $P_y = (a-b)^*(a-b)/2 = 1 - (a^*b + b^*a)/2$, $P_+ = a^*a$, and $P_- = b^*b$. The polarizations are then $P_{lin} = (P_x - P_y)/(P_x + P_y) = a^*b + b^*a$ and $P_{circ} = (P_+ - P_-)/(P_+ + P_-) = a^*a - b^*b$. If we let $a = \alpha e^{i\theta}$ and $b = \beta e^{i\phi}$, then $\alpha^2 + \beta^2 = 1$. Let $\alpha = \cos\gamma$

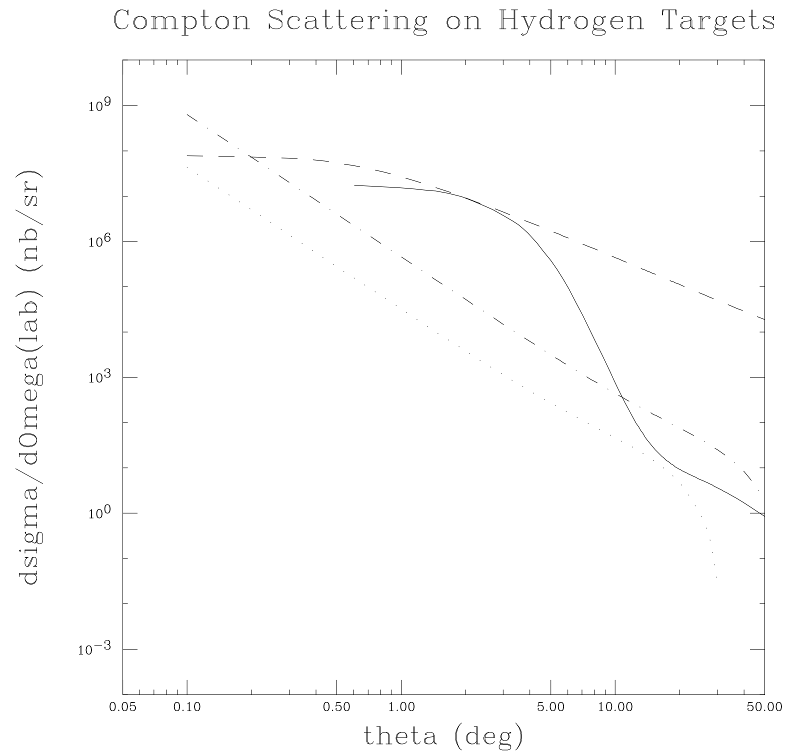

Figure 7: Compton scattering from hydrogen targets with a $k = 3$ GeV beam. See text for explanation of the curves.

and $\beta = \sin\gamma$. Then $P_{lin} = 2\alpha\beta\cos(\theta - \phi) = \sin 2\gamma \cos(\theta - \phi)$ and $P_{circ} = \alpha^2 - \beta^2 = \cos 2\gamma$. If $P_{circ} = \pm 1$ then $P_{lin} = 0$. The ratio $P_{lin,max}/P_{circ} = \tan 2\gamma$. Therefore, for $P_{circ} = 0.3, 0.5, 0.7,$ and 0.9, $P_{lin,max} = 0.95, 0.87, 0.71,$ and 0.44, respectively. For a given P_{circ}, P_{lin} ranges from $-P_{lin,max}$ to $P_{lin,max}$.

References

[1] G. Buschhorn, *et al.*, Phys. Lett. **B33**(1970)241; Phys. Lett. **B37**(1971)211.

[2] S.J. Brodsky and G.R. Farrar, Phys. Rev. Lett. **31**(1973)1153.

[3] M. Deutsch, *et al.*, Phys. Rev. D **8**(1973)3828.

[4] M.A. Shupe, *et al.*, Phys. Rev. D **19**(1979)1921.

[5] J. Duda, *et al.*, Z. Phys. **C17**(1983)319.

[6] A.M. Breakstone, *et al.*, Phys. Rev. Lett. **47**(1981)1778.

[7] A.M. Boyarski, *et al.*, Phys. Rev. Lett. **26**(1971)1600.

[8] R.L. Anderson, *et al.*, Phys. Rev. Lett. **25**(1970)1218.

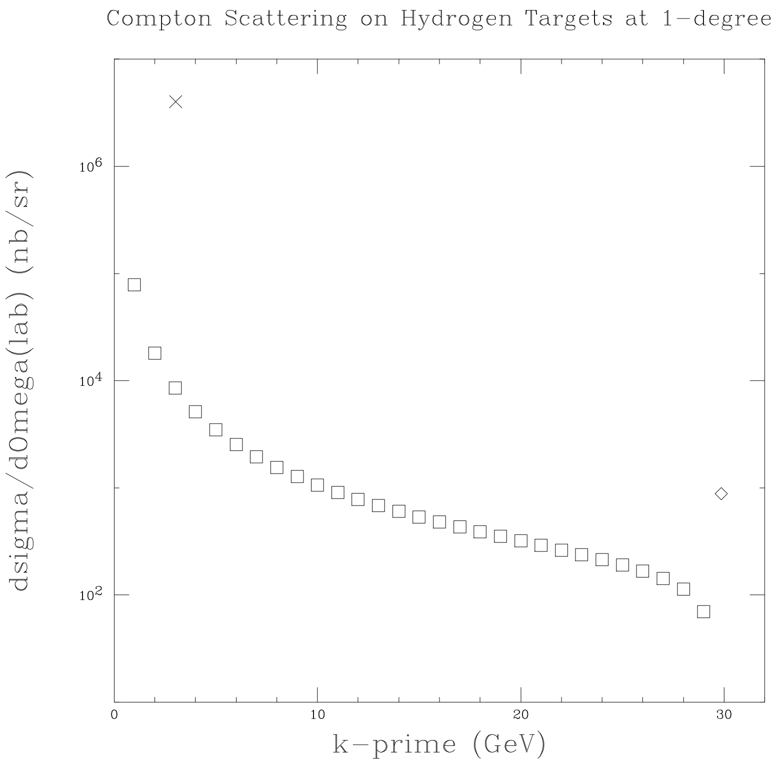

Figure 8: Compton cross sections for $\theta_{lab} = 1°$ as a function of scattered photon energy. See text for expanation of the points.

[9] Jefferson Lab Proposal E97-108, B. Wojtsekhowski and C. Hyde-Wright (spokespersons), 1998, unpublished.

[10] H.A. Tolhoek, Rev. Mod. Phys. **28**(1956)277.

[11] E. Maël, Z. Phys. **C61**(1994)83.

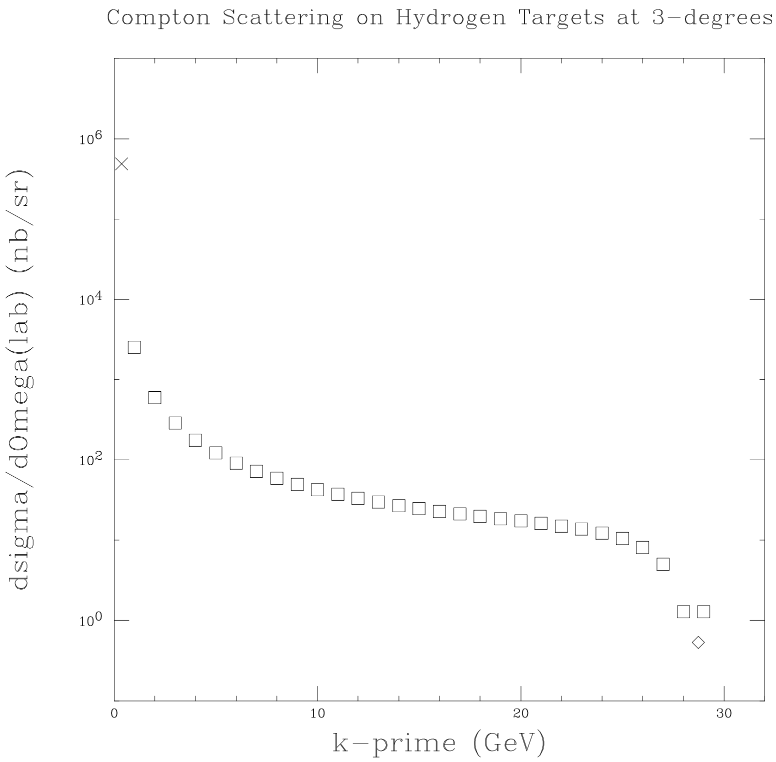

Figure 9: Compton cross sections for $\theta_{lab} = 3°$ as a function of scattered photon energy. See text for expanation of the points.

Table 10: Deep-inelastic Compton scattering rates for a 1 b^{-1} target, 10^7 photons per second for a month of continuous running. The bins are $\Delta\theta = 1°$, and $\Delta k' = 1$ GeV.

θ (deg)	Q^2 GeV^2	X'_T	x	σ_{DIS} (nb/sr/GeV)	A	counts	dA	$dA/A \times 100$
3	1.25	0.21	0.05	24.42	0.17	4204	0.02	9
4	2.22	0.28	0.08	11.91	0.25	2732	0.02	8
5	3.47	0.35	0.12	6.75	0.33	1935	0.02	7
6	5.00	0.42	0.18	4.07	0.41	1399	0.03	6
7	6.80	0.49	0.24	2.48	0.50	995	0.03	6
8	8.88	0.56	0.32	1.48	0.60	677	0.04	6
9	11.23	0.63	0.40	0.83	0.70	427	0.05	7
10	13.86	0.70	0.50	0.42	0.80	241	0.06	8
11	16.76	0.77	0.60	0.18	0.90	113	0.09	10
12	19.93	0.84	0.72	0.06	1.00	38	0.16	16